Supporting Information

Biomineralization-Driven Ion Gate in TiO_2 Nanochannel Arrays for Cell H_2S Sensing

Junli Guo[†], Lingling Yang[†], Huijie Xu[†], Chenxi Zhao[†], Zhenqing Dai[†], Zhida Gao [†], and Yanyan Song [†,*]

† College of Sciences, Northeastern University, Box 332, Shenyang 110004, China

* Corresponding emails: yysong@mail.neu.edu.cn

Table of Content:

1. Apparatus

2. Figures

Figure S1. The affinity interaction between BSA and TiO_2M.

Figure S2. *I-V* curves at different KCl concentrations.

Figure S3. UV-Vis spectra and FTIR spectra of BSA modification.

Figure S4. *I-V* curves for optimizing the absorption time of Cu^{2+}.

Figure S5. Zeta potential after each modification step.

Figure S6. Calibration plot of I/I_0 versus the logarithm of the S^{2-} concentration.

Figure S7. *I-V* curves of TiO_2-BSA-Cu^{2+} after react with S^{2-} in the Tris-HCl buffer with different pH values.

Table S1. The EDS analysis of TiO_2M-BSA-CuS.

Figure S8. *I-V* profiles before and after the reaction of various anions.

Figure S9. *I-V* profiles before and after the reaction of various inorganic sulfur species and biothiols.

Figure S10. Optimized time of cell incubation.

Figure S11. Calibration curves and UV-vis spectra of H_2S detection using methylene blue assay.

1. Apparatus

The UV-vis absorption spectra were obtained by means of Perkin–Elmer, spectrometer (Lambda XLS+, USA). The morphological characterization was carried out on a field-emission scanning electron microscope (Hitachi FE-SEM SU8000, Japan) and atomic force microscope (Bruker AFM Dimension Icon, USA). The crystal structures were identified by Powder X-ray diffraction (XRD) patterns, which were collected using an X'Pert X-ray diffraction spectrometer (Philips, USA) using a CuKα X-ray source. Fourier transform infrared spectroscopy (FTIR) was performed on a Nicolet 6700 instrument (ThermoFisher, USA). The zeta potentials of nanochannels were measured on a Zetasizer Nano ZS90 analyzer (Malvern, USA). The CHI660D electrochemical workstation (CH Instrument Co. Shanghai) was used for all electrochemical tests with two Ag/AgCl electrodes as the anode and cathode.

2. Figures

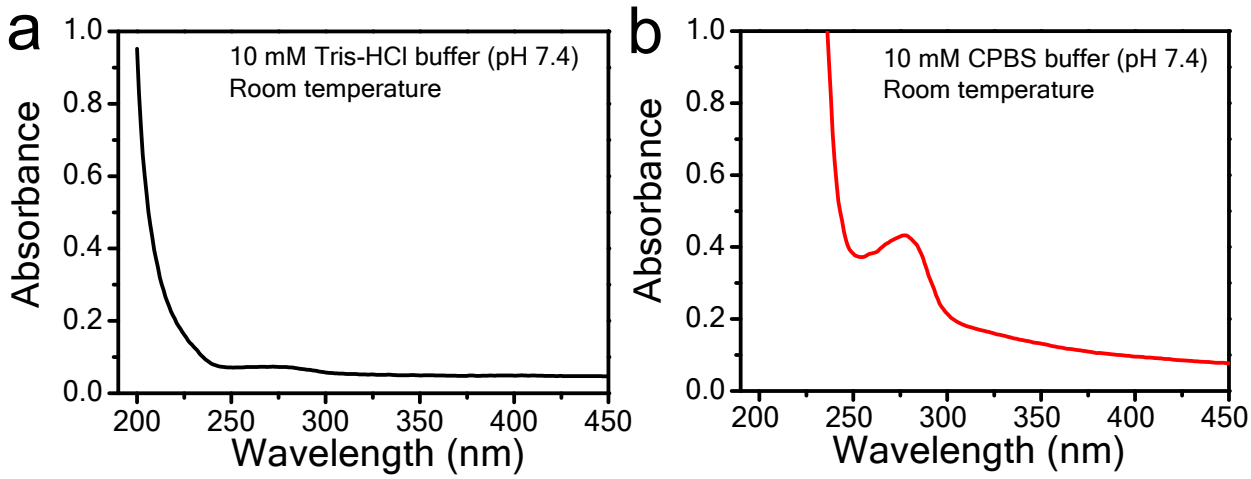

Figure S1. UV-vis absorption spectra of (a) 10 mM Tris-HCl buffer (pH 7.4) and (b) 10 mM sodium citrate buffer (pH 7.4) solution after TiO_2M-BSA samples were incubated in each solution for 4 h.

Compared to the absorption spectrum of Tris-HCl buffer (Figure S1a), an obvious absorption peak of BSA appeared after the incubation of TiO_2M-BSA in sodium citrate buffer (Figure S1b), suggesting the adsorbed BSA molecules were displaced by the citrate in the buffer. This result indicated the BSA molecules were anchored on the TiO_2 surface by the bidentate interaction between carboxyl groups on BSA and hydroxyl groups on amorphous TiO_2.

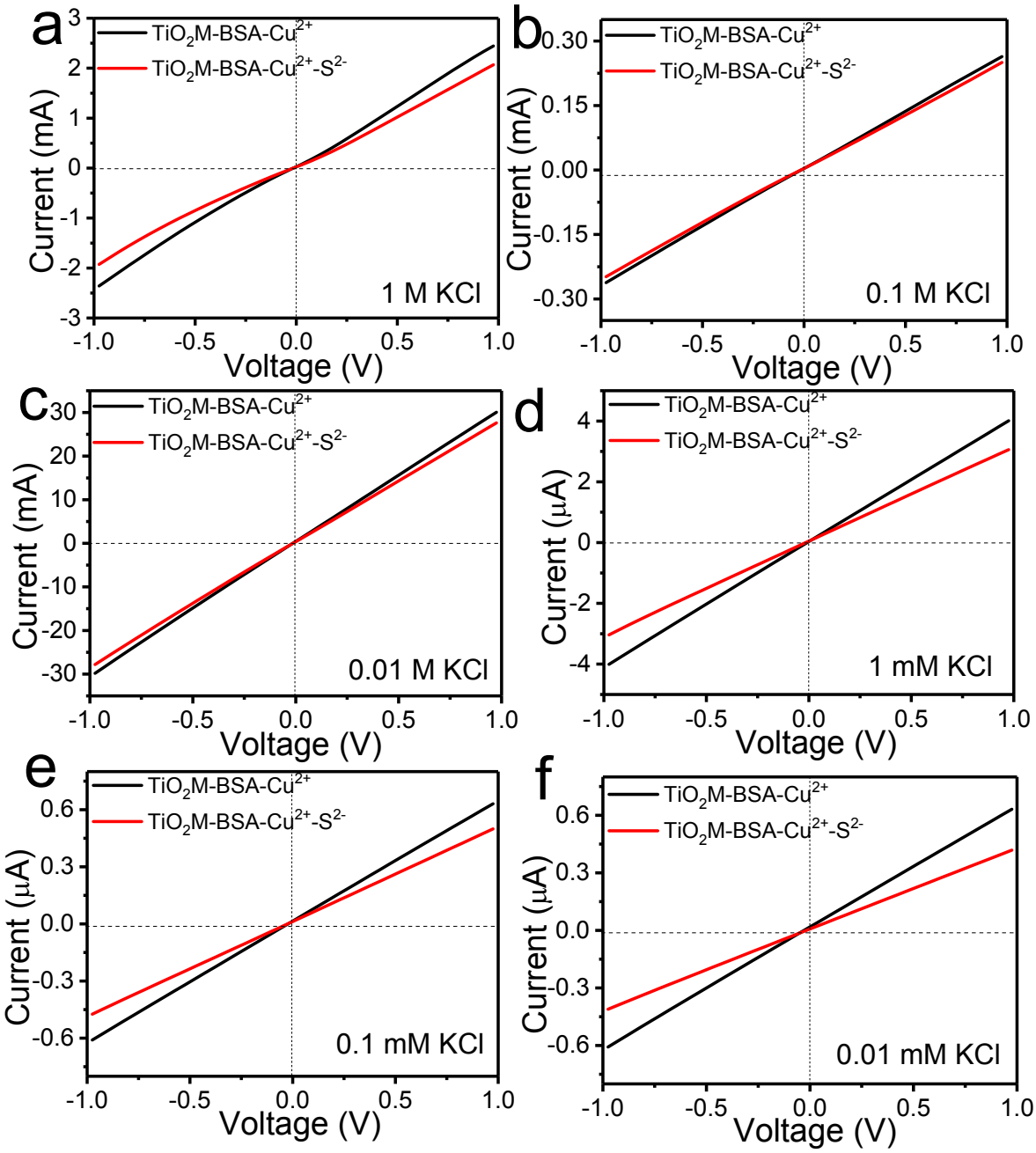

Figure S2. *I-V* curves at different KCl concentrations. Scan rate: 50 mV/s.

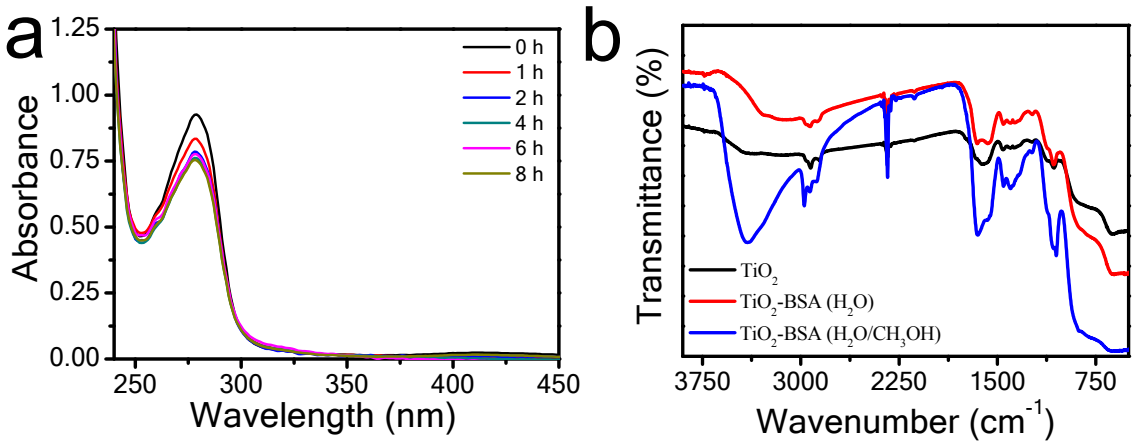

Figure S3. (a) UV-Vis spectra of the optimized BSA adsorption. (b) FTIR before and after modification of BSA.

For FTIR spectra, the amide I and amide II bands are indicative of a predominant structural contribution from α-helices structure of the protein. Methanol produces three major effects on protein structure: i) destruction of rigid native structure, ii) induction of α-helical structure, and iii) dissolution of peptide or its aggregates. More α-helix of BSA thus can be exposed in a methanol contained solvent. It can be noticed in Figure S3b that IR peaks for the amide I (*ca.* 1650 cm^{-1}) and amide II (*ca.* 1555 cm^{-1}) presented a higher intensity for the sample that was prepared in methanol-water solvent than the sample prepared in the pure water.

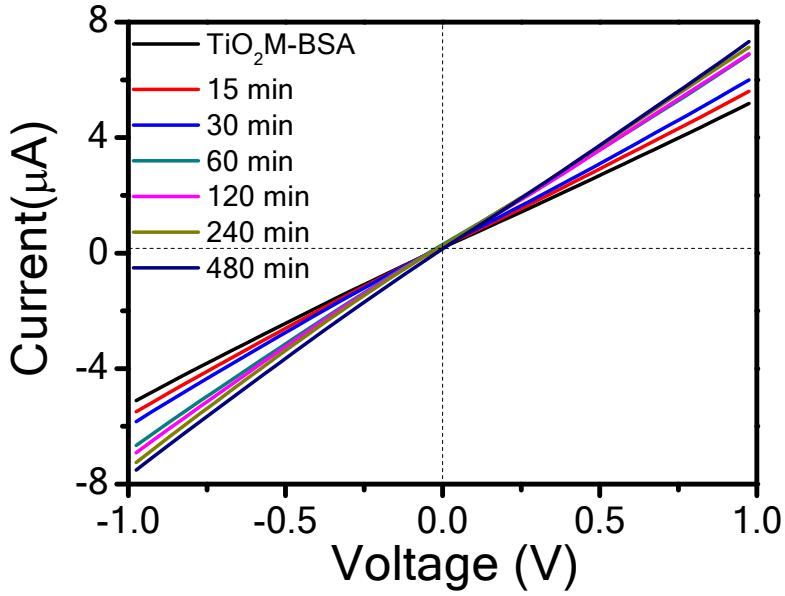

Figure S4. The influence of Cu^{2+} adsorption time on the *I-V* properties TiO_2M-BSA.

The optimized adsorption time to form TiO_2M-BSA-Cu^{2+} was 4 h.

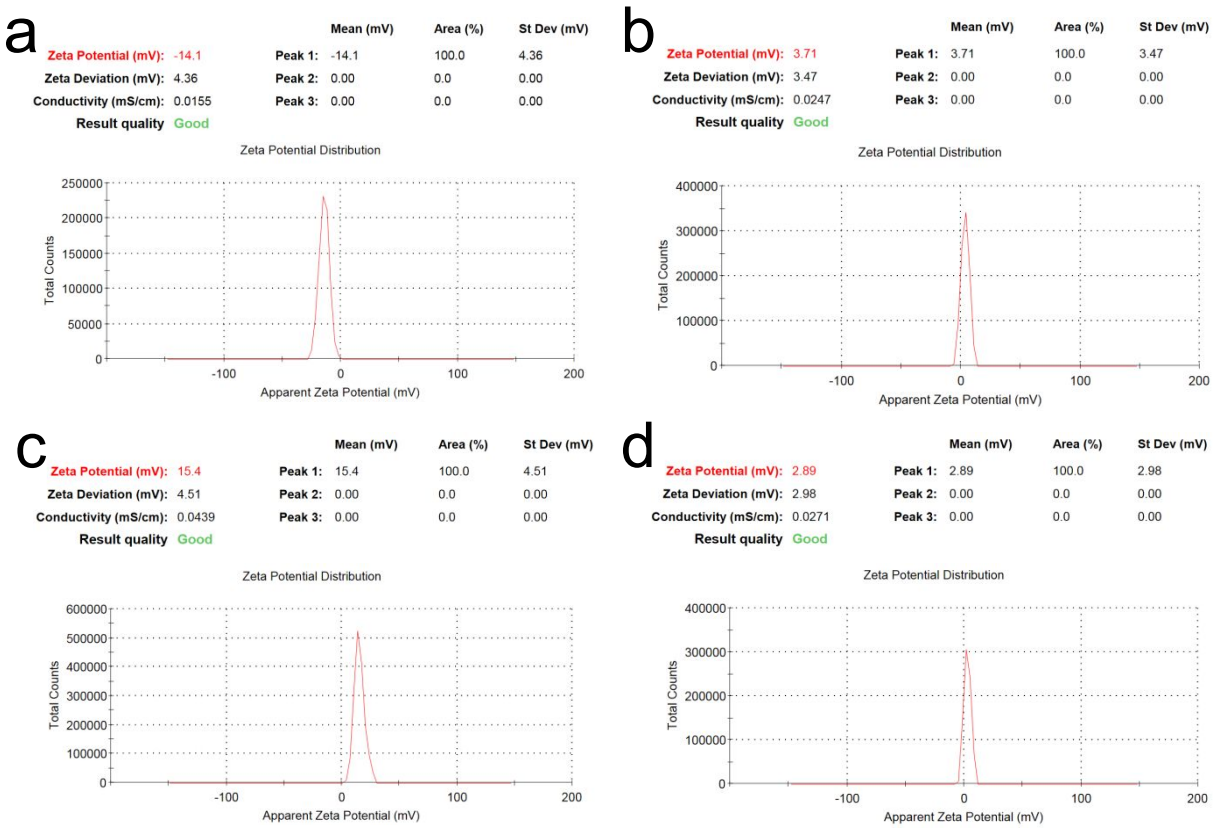

Figure S5. Zeta potentials of TiO_2M, TiO_2M-BSA, TiO_2M-BSA-Cu^{2+}, and TiO_2M-BSA-CuS.

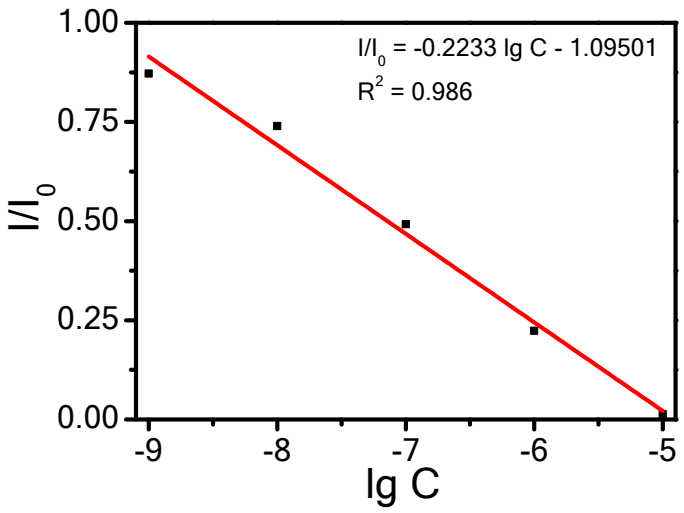

Figure S6. Calibration plot of I/I_0 at + 1.0 V versus the logarithm of the S^{2-} concentration.

The detection limit was estimated to be 1.0 nM by a 3 SD/L method (where SD is the standard deviation of the blank and L is the slope of the calibration curve).

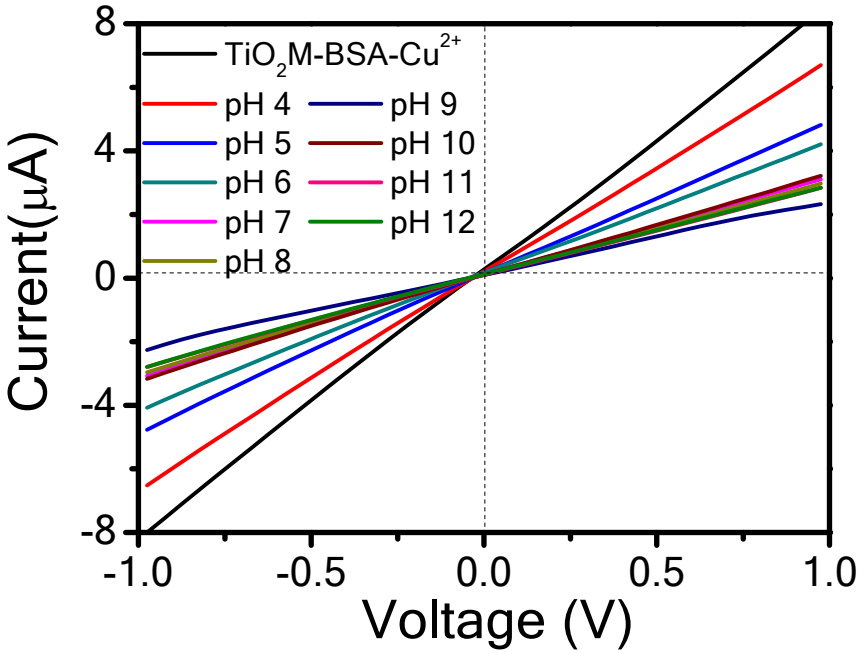

Figure S7. *I-V* curves of TiO_2-BSA-Cu^{2+} before and after react with S^{2-} in the Tris-HCl buffer with different pH values.

Element	Weight %	Atomic %
C K	6.68	13.39
O K	39.65	59.61
S K	0.84	0.63
Ti K	51.48	25.86
Cu K	1.35	0.51

Table S1. The EDS analysis of TiO_2M-BSA-CuS.

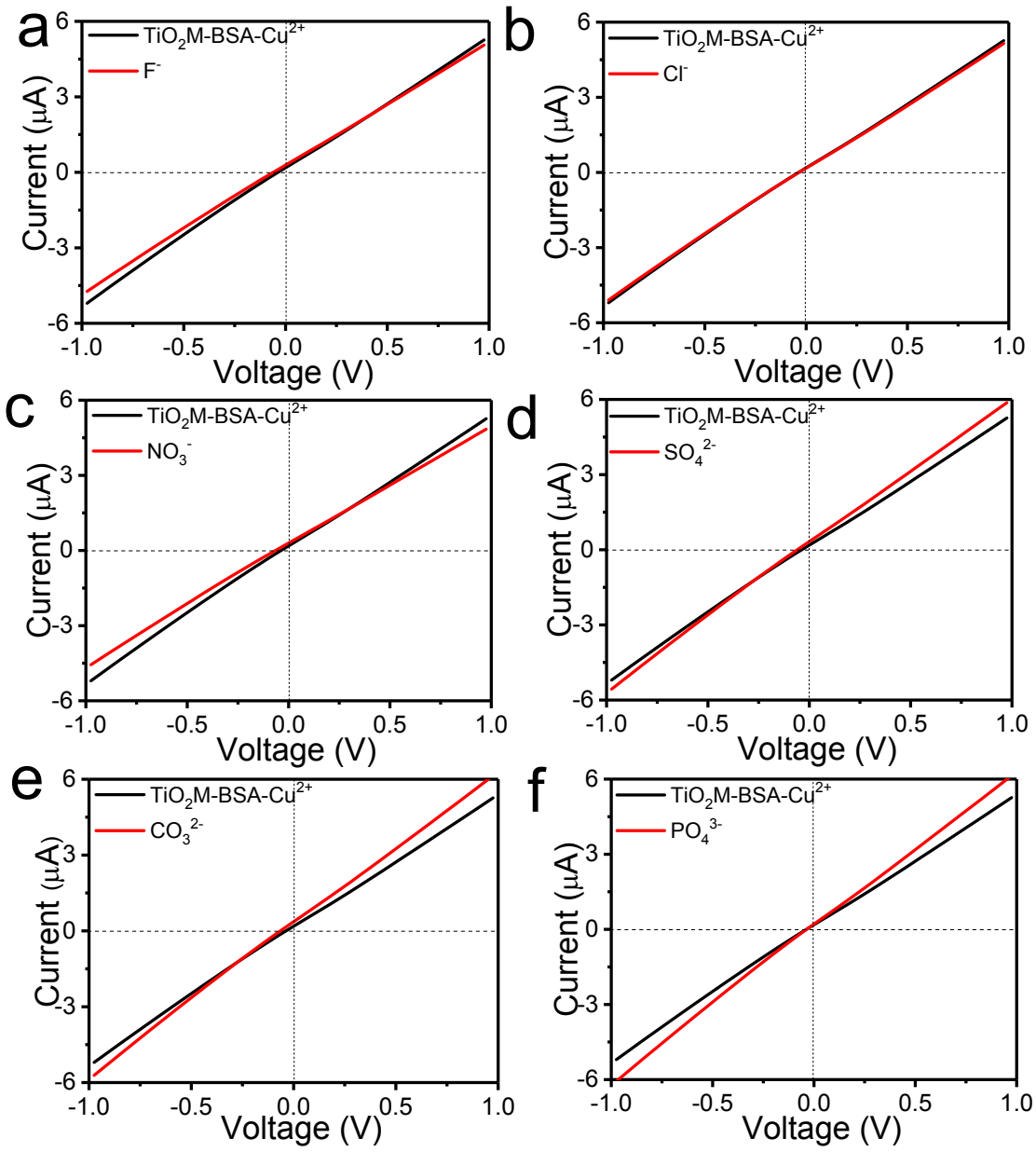

Figure S8. *I-V* profiles before and after the reaction of various anions.

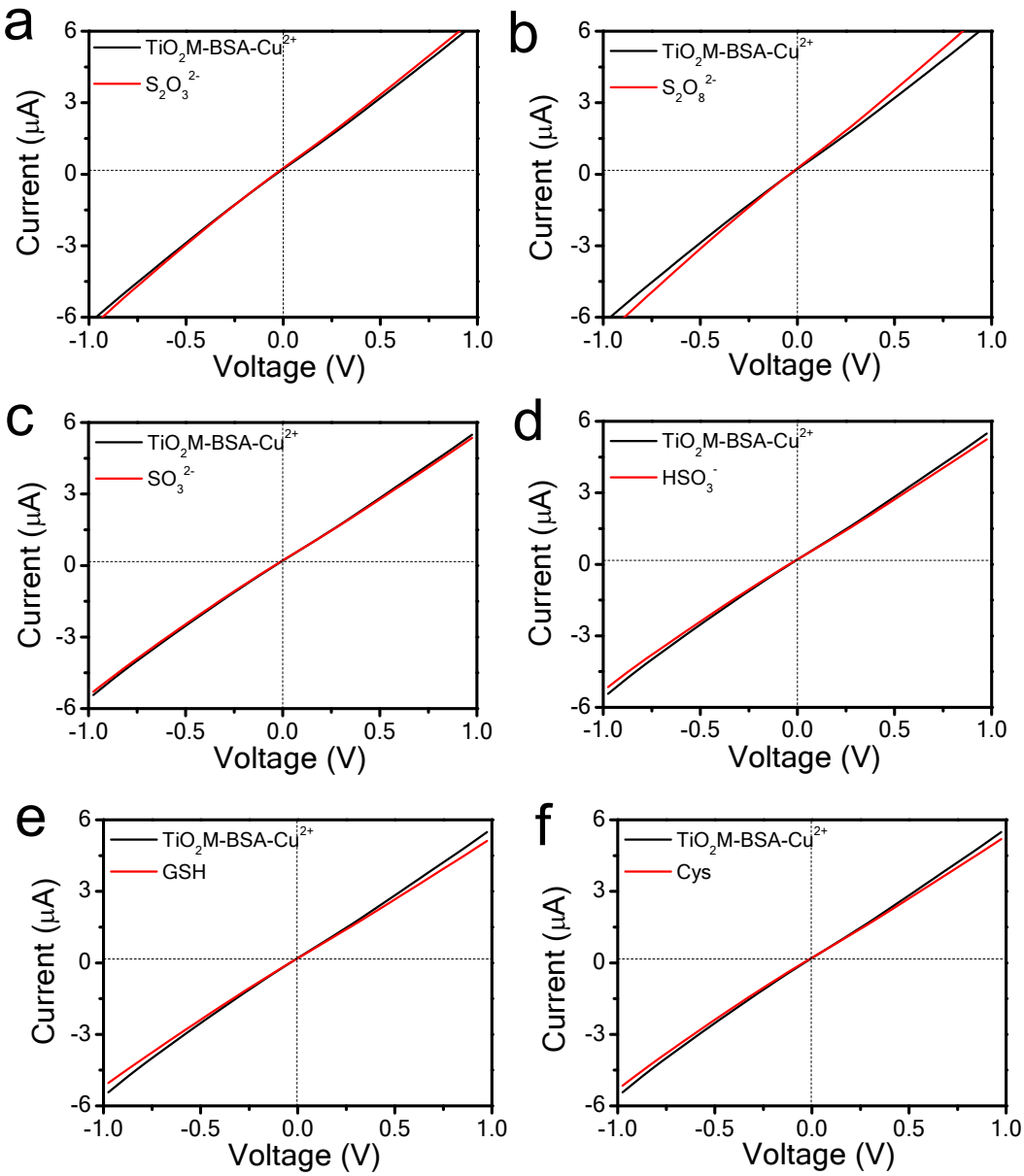

Figure S9. *I-V* profiles before and after the reaction of various inorganic sulfur species and biothiols.

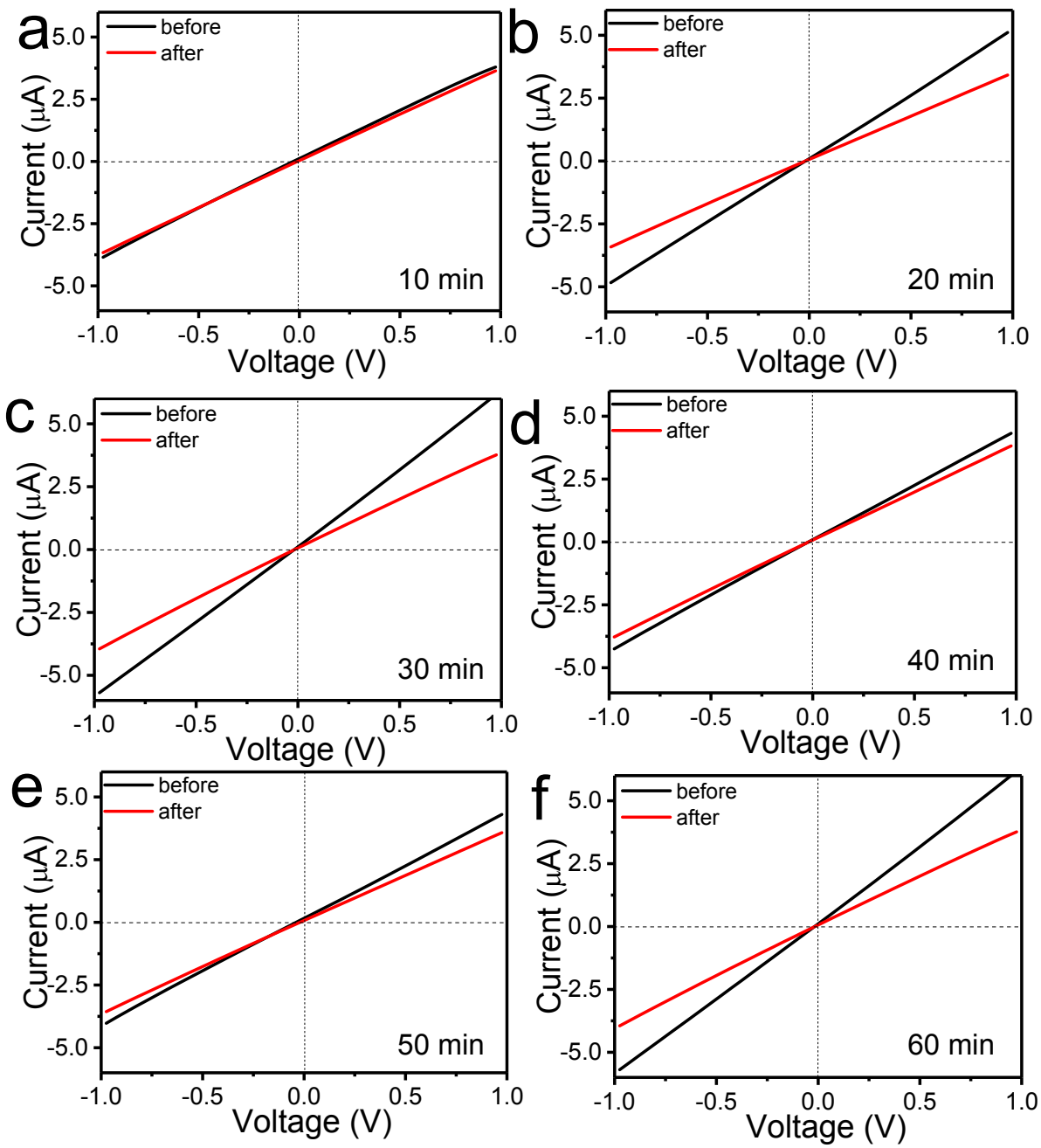

Figure S10. The influence of TiO_2M incubation time on cytosensory current (S^{2-} was released from 56 MCF-7 cells).

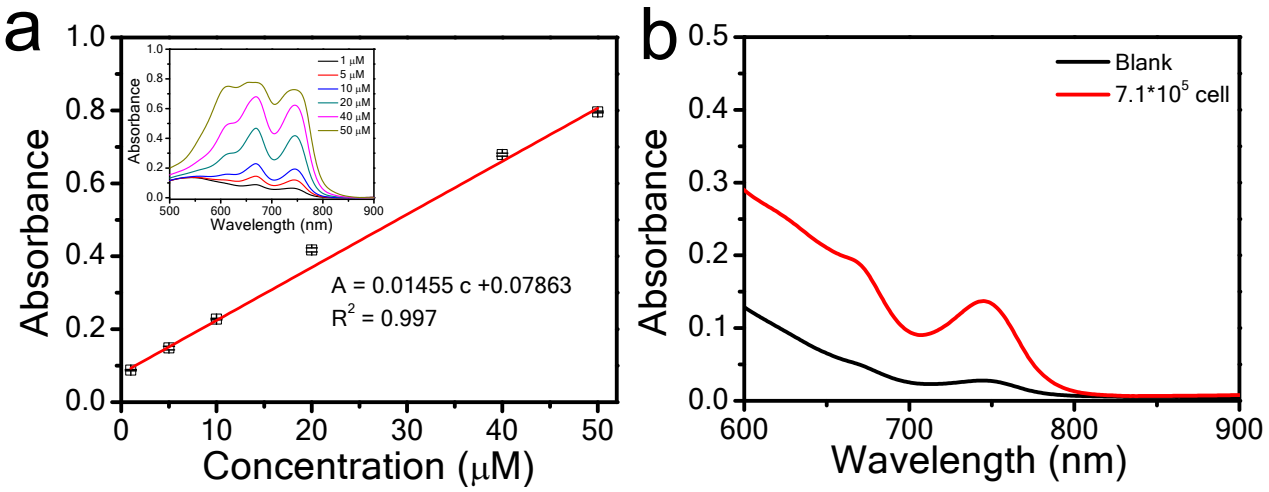

Figure S11. (a) Calibration curves of the absorbance at 670 nm versus concentration of Na_2S (Inset: UV-vis spectra of different concentrations of Na_2S). (b) UV-vis absorption spectra of the MB generated by H_2S from 7.1×10^5 cells.

The detection limit of the MB method is estimated to be 0.81 μM by a 3 SD/L method.

Reference

(1) Huai, Q.; He, Y.; Sheng, F.; Tao, Z. Effects of pH and Metal Ions on the Conformation of Bovine Serum Albumin in Aqueous Solution - An Attenuated Total Reflection (ATR) FTIR Spectroscopic Study. *Spectrochimica Acta Part A* **1996**, *52*, 1795-1800.

(2) Lin, S. Y.; Wei, Y. S.; Li, M. J.; Wang, S. L. Effect of Ethanol or/and Captopril on the Secondary Structure of Human Serum Albumin Before and After Protein Binding. *European Journal of Pharmaceutics & Biopharmaceutics* **2004**, *57*, 457-464.